peared to have bounded dispersive errors. It has been found that the best overall performance is achieved by Osher-Chakravarthy third-order limiter.

Acknowledgments

This work was performed as a part of SBIR Phase II project sponsored by NASA MSFC under a SBIR Phase II contract. The authors are grateful to Paul McConnaughey of NASA MSFC, and to S. Venkateswaran of Penn State University for supplying the analytical solution for the combustion instability problem.

References

[1]Harten, A., "High-Resolution Schemes for Hyperbolic Conservation Laws," *Journal of Computational Physics*, Vol. 49, No. 2, 1983, pp. 357–393.

[2]Chakravarthy, S. R., and Osher, S., "A New Class of High-Accuracy TVD Schemes and Their Applications," *Journal of Computational Physics*, Vol. 68, No. 1, 1987, pp. 151–179.

[3]Yee, H. C., "A Class of High-Resolution Explicit and Implicit Shock-Capturing Methods," NASA TM-101088, Feb. 1989.

[4]Roe, P. L., "Approximate Riemann Solvers, Parameter Vectors and Difference Schemes," *Journal of Computational Physics*, Vol. 43, No. 2, 1981, pp. 357–372.

[5]Priem, R. J., "Round Robin Calculation of Wave Characteristics in a Fixed Geometry-Operating Conditions Liquid Rocket Using Given Simplified Combustion Equations," JANNAF Workshop on Numerical Methods in Combustion Instability, Orlando, FL, Feb. 1990.

[6]Venkateswaran, S., Grenda, J., and Merkle, C. L., "Computational Fluid Dynamic Analysis of Liquid Rocket Combustion Instability," *Proceedings of the AIAA 10th Computational Fluid Dynamics Conference* (Honolulu, HI), AIAA, Washington, DC, 1991, pp. 926–936.

Effect of Imposed Pressure Gradients on the Viscous Stability of Longitudinal Vortices

Robert E. Spall*
University of South Alabama, Mobile, Alabama 36688

I. Introduction

VISCOUS stability calculations of the "q-vortex" [derived from the far-wake solution for a trailing line vortex (Batchelor[1])] have been performed by Lessen and Paillet,[2] Stewartson,[3] and Khorrami.[4] Several other researchers have investigated the inviscid stability of these profiles (Lessen et al.,[5] Duck and Foster,[6] Leibovich and Stewartson,[7] Stewartson and Capell,[8] Duck[9]). Results show that the stability of the vortex is strongly dependent on the value of q (related to the ratio of the maximum swirl velocity to the maximum axial velocity). For instance, the vortex is completely stabilized to inviscid disturbances for values of $q > 1.5$, with the most unstable wave obtained in the limit $|n| \to \infty$ (where n is the azimuthal wave number).

In the present work, the effects of pressure gradients on the viscous stability of longitudinal vortices are investigated. Mean flow profiles computed as numerical solutions to the quasicylindrical equations of motion are employed. This procedure allows one to impose pressure gradients through the boundary conditions at the radial edge of the domain. To this author's knowledge, the effect of imposed pressure gradients on the stability of longitudinal vortices has not yet been studied.

The stability calculations are performed using a normal mode analysis. Although, strictly speaking, a nonparallel stability theory is appropriate [multiple scales (Saric and Nayfeh[10]) or parabolized stability equation approach (Bertolotti[11])], the quasiparallel flow assumption is made. The quasiparallel assumption is justified on the grounds that the spatial development of the vortex is relatively slow; that is, at high Reynolds numbers and under the influence of weak pressure gradients, significant changes occur over many wavelengths. Provisions are made to include some nonparallel effects by retaining radial velocity and streamwise derivative terms in the mean flow. The stability formulation is based on second-order-accurate finite difference approximations on a staggered grid, with the accuracy of the computed eigenvalues being improved through Richardson extrapolation.

II. Problem Formulation

Mean Flow

The linear stability of solutions to the quasicylindrical equations of motion is considered. The quasicylindrical equations are derived from the laminar, incompressible, axisymmetric equations of motion as a result of boundary-layer-type assumptions (Hall[12]) and are given as

$$\frac{\partial u}{\partial r} + \frac{u}{r} + \frac{\partial w}{\partial z} = 0 \tag{1}$$

$$\frac{v^2}{r} = \frac{\partial p}{\partial r} \tag{2}$$

$$u\frac{\partial v}{\partial r} + \frac{uv}{r} + w\frac{\partial v}{\partial z} = \frac{1}{Re}\left(\frac{\partial^2 v}{\partial r^2} + \frac{1}{r}\frac{\partial v}{\partial r} - \frac{v}{r^2}\right) \tag{3}$$

$$u\frac{\partial w}{\partial r} + w\frac{\partial w}{\partial z} = -\frac{\partial p}{\partial z} + \frac{1}{Re}\left(\frac{\partial^2 w}{\partial r^2} + \frac{1}{r}\frac{\partial w}{\partial r}\right) \tag{4}$$

where r and z are cylindrical-polar coordinates; u, v, and w are the radial, swirl, and axial velocity components; p is the pressure, and Re is the Reynolds number. Lengths have been made nondimensional with respect to a length scale l [defined following Eq. (11)], velocities with respect to a velocity scale W_∞, and pressure with respect to ρW_∞^2.

The preceding equations are solved subject to the following boundary conditions:

$$\text{at } r = 0: \quad u = v = \frac{\partial w}{\partial r} = 0 \tag{5}$$

$$\text{at } r = r_0: \quad v = V(z); \qquad w = W(z); \qquad p = P(z) \tag{6}$$

In addition, initial conditions are specified at $z = 0$ as

$$v = v_0(r) \tag{7}$$

$$w = w_0(r) \tag{8}$$

which are derived from Eqs. (10) and (11) later.

In general, the specification of the outer boundary conditions and the radius of the outer boundary may be arbitrarily specified. An exception occurs if the outer boundary represents an inviscid stream surface. In that case, the relationship

$$\frac{u}{w} = \frac{dr}{dz} \tag{9}$$

is implied and only one of r_0, W, or P may be arbitrarily specified. An iterative solution procedure is then implemented such that r_0 takes on a value appropriate for the stream surface defined by Eq. (9). This is the procedure followed in this paper for the pressure gradient cases. That is, the pressure is specified along the outer boundary, which is defined as an inviscid stream surface. The problem is parabolic in the streamwise direction and thus the equations may be solved by marching in z. The quasicylindrical equations were first solved by Hall[13]

Received March 9, 1993; revision received July 26, 1993; accepted for publication Aug. 17, 1993.

*Assistant Professor, Mechanical Engineering.

using finite difference methods for several sets of initial and boundary conditions.

The objective of the present study is to investigate the linear stability of a longitudinal vortex under the effect of a weak pressure gradient. Toward this end, initial conditions are derived from the similarity solution to the trailing line vortex[1] and are given in dimensionless form as

$$v = \frac{\hat{q}}{r}(1 - e^{-(1.122r)^2}) \tag{10}$$

$$w = 1 + \delta e^{-(1.122r)^2} \tag{11}$$

where

$$\hat{q} = \frac{\sqrt{a}\lambda}{1.122 W_\infty}, \qquad \delta = \frac{W_0}{W_\infty}$$

λ and a are constants, and W_0 is the centerline axial velocity. The length scale was chosen as the vortex core radius (the radius at which the swirl velocity is a maximum), and thus

$$l = \frac{1.122}{\sqrt{a}}$$

The velocity scale was chosen as the far-field axial velocity W_∞.

The preceding equations are solved using second-order-accurate finite-difference approximations, marching in the streamwise direction. Grid resolutions used in the solution procedure were sufficient to ensure that the stability characteristics of the mean flow profiles are grid independent.

Stability Equations

Briefly, the stability equations are derived by first linearizing the equations of motion and then expressing the linearized perturbation variables in the form

$$\{u', v', w', p'\} = \{iF(r), G(r), H(r), P(r)\}e^{i(\alpha z + n\theta - \omega t)} \tag{12}$$

Here, α is the real axial wave number, n is the real azimuthal wave number, and ω is complex (thus, we are considering temporal stability). These equations, consisting of three second-order momentum equations and the continuity equation, have previously been given in Lessen and Paillet[2] and may be expressed in the form

$$(AD^2 + BD + C)\bar{\Phi} = 0 \tag{13}$$

where $\bar{\Phi}$ is a four element vector defined by $\bar{\Phi} = \{F, G, H, P\}^t$ and $D \equiv \partial/\partial r$ where r is the radial coordinate. The preceding equations are solved subject to the following boundary conditions[14]:

$$\text{at } r = 0, \quad \text{if } n = 0, \quad \Phi_1(0) = \Phi_2(0) = 0, \quad \Phi_3'(0) = 0 \tag{14a}$$

$$\text{if } n = \pm 1, \quad \Phi_1(0) \pm \Phi_2(0) = 0, \quad \Phi_1'(0) = 0, \quad \Phi_3(0) = 0 \tag{14b}$$

$$\text{if } |n| > 1, \quad \Phi_1(0) = \Phi_2(0) = \Phi_3(0) = 0 \tag{14c}$$

$$\text{as } r \to \infty, \quad \Phi_1 = \Phi_2 = \Phi_3 = 0 \tag{14d}$$

The solution technique employed is based on a second-order-accurate finite difference approximation on a staggered mesh. The staggered mesh eliminates the need for pressure boundary conditions. In addition, Richardson extrapolation is employed to increase the accuracy of the computed eigenvalues. The scheme is analagous to that employed quite successfully in the compressible boundary-layer stability code COSAL.[15] The discretized system represents, along with six boundary conditions, $4N + 3$ equations for $4N + 3$ unknowns (where N is the number of grid points). The system constitutes a generalized eigenvalue problem of the form

$$\hat{A}\bar{\Phi} = \hat{B}\omega\bar{\Phi} \tag{15}$$

which is solved for the eigenvalues ω using the IMSL QL routine CXLZ.

III. Results

The linear stability of solutions to the quasicylindrical equations of motion under the influence of weak pressure gradients is investigated. To provide a baseline for comparison, results for a zero pressure gradient case are examined first. The Reynolds number at the inflow plane Re_i was set to 1000 and the parameters $\hat{q}$ and δ were set to 0.5 and 1.0, respectively. Note that the Reynolds number is based on the local vortex core radius, and thus changes in the streamwise direction.

In the solution of the quasicylindrical equations for the mean flow, 400 points were used in the radial direction, with a stretching function employed to cluster points near the vortex core. The far-field boundary was set to $r_0 = 40$ (i.e., 40 core radii as defined at the inflow plane), and the streamwise step size was $\Delta z = 1$. The radius was chosen large enough so that the zero perturbation radial boundary conditions required for the solution of the stability equations would be satisfied.

Figure 1a shows the swirl velocity distribution as a function of radius for axial locations up to $z = 600$. This figure reveals that the vortex core has doubled in radius over an axial distance of $z = 600$, and that at this location, the maximum swirl velocity has decreased to $\approx 50\%$ of that at inflow. The corresponding axial velocity profiles are shown in Fig. 1b. Note that the jetlike profile still exists at $z = 600$. Clearly, decay due to laminar diffusion is a slow process (in relation to other physical mechanisms such as vortex breakdown or turbulent diffusion) and thus provides much of the incentive for studying the stability of these vortices. This also provides some justification for the quasiparallel stability formulation.

Figure 2a shows growth rate curves for the preceding mean flow as a function of wave number as the vortex evolves in

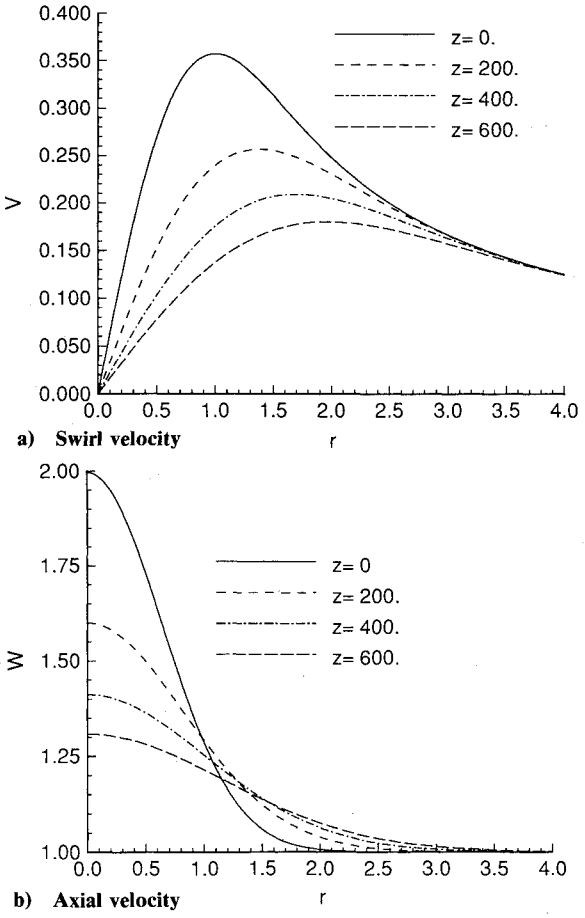

Fig. 1 Mean flow solutions computed as solutions to the quasicylindrical equations of motion; $Re_i = 1000$, $\hat{q} = 0.5$, $\delta = 1.0$.

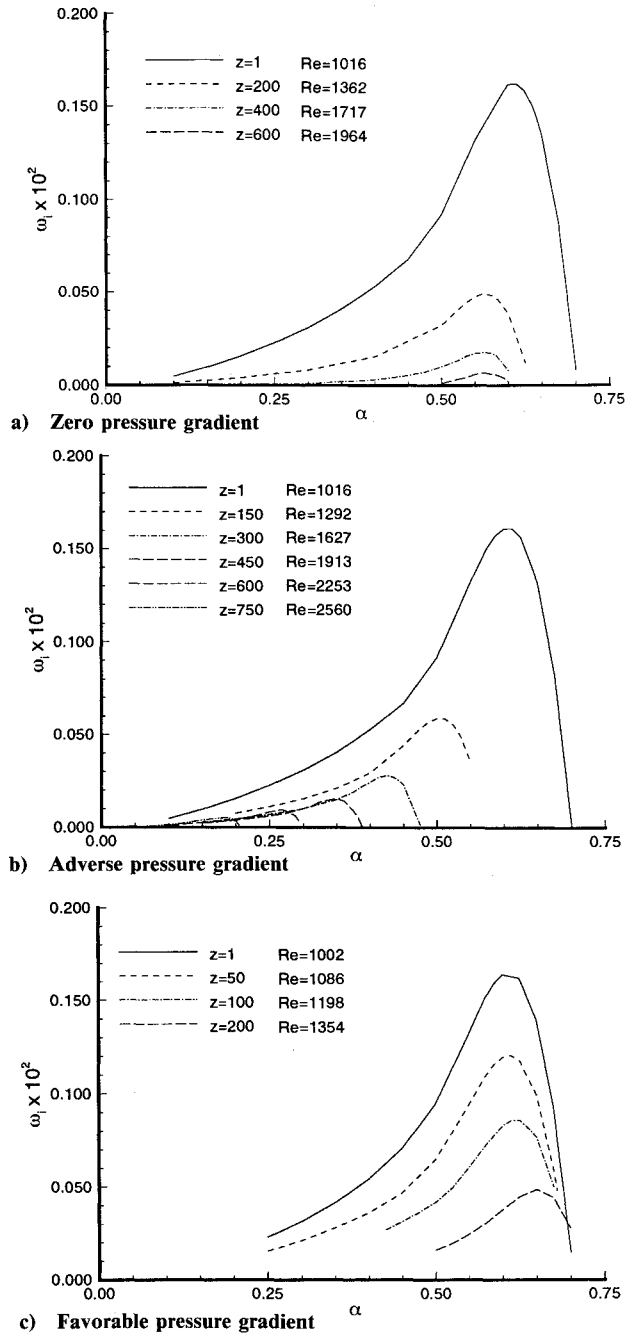

Fig. 2 Growth rate as a function of wave number at various streamwise locations.

space; i.e., for $z = 1$, 200, 400, and 600 (corresponding to local Reynolds numbers of 1016, 1362, 1717, and 1964, respectively). A substantial decrease in the maximum growth rates is observed as the vortex evolves. This decrease is due primarily to a decrease in the local swirl ratio (the magnitude of which may be acertained from Fig. 1a). Based on the results of Khorrami,[4] the increase in local Reynolds number may be expected to have a minor stabilizing effect. The figure also indicates that the most unstable wave number remains nearly constant at $\alpha \approx 0.575$. It is noted that a search over a wide range of wave numbers failed to reveal any instability for axisymmetric ($n = 0$) modes.

We now investigate the effect of favorable and adverse pressure gradients on the stability characteristics of the vortex. Mean flows are computed for pressure gradients specified as $\partial p/\partial z = \pm 0.0005$ (imposed along the outer boundary stream tube). The other parameters are identical with those of the zero pressure gradient case. The stability results for the adverse pressure gradient are shown in Fig. 2b, and results for the favorable pressure case are shown in Fig. 2c. Figure 2b indicates that the adverse gradient has only a minimal effect on the maximum growth rates of the vortex (when compared to the zero pressure gradient case). However, the most unstable modes rapidly shift toward longer wavelength disturbances (the α corresponding to the highest growth rate decreases from 0.6 at $z = 0$ to 0.18 at $z = 750$), with the shorter wavelength disturbances becoming stable.

Results shown in Fig. 2c indicate that the effects of the favorable gradient on the maximum growth rates of the vortex are minimal. However, in this case the maximum growth rates shift toward shorter wavelength disturbances as the vortex evolves in the streamwise direction. The longer wavelength disturbances also remain unstable. It is noted that a search failed to reveal any viscous instability of the $n = 0$ mode for either the favorable or adverse pressure gradient cases (for the given values of $\hat{q}$ and δ).

The preceding calculations were made using the quasiparallel flow approximation. Additional calculations were performed that included nonparallel terms in the mean flow profiles. That is, stability results were also obtained by including terms containing the radial velocity, and streamwise derivative of the axial velocity, in the coefficient matrix [of Eq. (15)]. Although plots are not presented, the results are worth mentioning. The primary effects are in terms of the growth rates. That is, for the adverse pressure gradient case, at some downstream location, the growth rates begin to increase. Conversely, for the favorable pressure gradient case, the growth rates were decreased (compared with the results in Fig. 2c) as the vortex evolved. The trends concerning the shift in wavelengths of the most unstable modes remained unchanged. A properly formulated nonparallel analysis would be required to verify these findings, which have implications in areas such as vortex breakdown.

IV. Conclusions

The linear stability of a quasicylindrical vortex evolving in the streamwise direction was investigated. The mean flow profiles were computed as numerical solutions to the quasicylindrical equations of motion with imposed pressure gradients. Results indicate that, under the quasiparallel approximation, the maximum growth rates of the vortex are not greatly influenced by pressure gradients. However, under the influence of an adverse pressure gradient, the most unstable disturbances rapidly shifted toward longer wavelengths as the vortex evolved in the streamwise direction. In all cases, viscous disturbances were noted only for the $n = 1$ mode. Further work into the stability of these swirling flows is anticipated by the author. To properly account for nonparallel effects, a multiple-scale technique will be attempted.

Acknowledgments

The author would like to acknowledge the NASA JOVE program and the Alabama Supercomputer Authority for providing the necessary resources.

References

[1]Batchelor, G. K., "Axial Flow in Trailing Line Vortices," *Journal of Fluid Mechanics,* Vol. 20, 1964, pp. 645–658.

[2]Lessen, M., and Paillet, F., "The Stability of a Trailing Line Vortex. Part 2. Viscous Theory," *Journal of Fluid Mechanics,* Vol. 65, 1974, pp. 769–779.

[3]Stewartson, K., "The Stability of Swirling Flows at Large Reynolds Numbers When Subjected to Disturbances at Large Azimuthal Wavenumber," *Physics of Fluids,* Vol. 25, Nov. 1982, pp. 1953–1957.

[4]Khorrami, M., "On the Viscous Modes of Instability of a Trailing Line Vortex," *Journal of Fluid Mechanics,* Vol. 225, 1991, pp. 197–212.

[5]Lessen, M., Singh, P. J., and Paillet, F., "The Stability of a Trailing Line Vortex. Part 1. Inviscid Theory," *Journal of Fluid Mechanics,* Vol. 63, 1974, pp. 753–763.

[6]Duck, P. W., and Foster, M. R., "The Inviscid Stability of a Trailing Line Vortex," *Journal of Applied Mathematics and Physics,*

Vol. 31, 1980, pp. 523-530.

[7]Leibovich, S., and Stewartson, K., "A Sufficient Condition for the Instability of Columnar Vortices," *Journal of Fluid Mechanics,* Vol. 126, 1983, pp. 335-356.

[8]Stewartson, K., and Capell, K., "On the Stability of Ring Modes in a Trailing Line Vortex: the Upper Neutral Points," *Journal of Fluid Mechanics,* Vol. 156, 1985, pp. 369-386.

[9]Duck, P., "The Inviscid Stability of Swirling Flows: Large Wavenumber Disturbances," *Journal of Applied Mathematics and Physics,* Vol. 37, May 1986, pp. 340-360.

[10]Saric, W. S., and Nayfey, A. H., "Nonparallel Stability of Boundary-Layer Flows," *Physics of Fluids,* Vol. 8, Aug. 1975, pp. 945-950.

[11]Bertolotti, F. P., "Compressible Boundary Layer Stability Analyzed With the PSE Equations," AIAA 22nd Fluid Dynamics, Plasma Dynamics and Lasers Conference, AIAA Paper 91-1637, Honolulu, HI, June 1991.

[12]Hall, M. G., "Vortex Breakdown," *Annual Review of Fluid Mechanics,* Vol. 4, 1972, pp. 195-218.

[13]Hall, M. G., "A Numerical Method for Solving the Equations for a Vortex Core," Royal Aircraft Establishment, Tech. Rept. No. 65106, Farnborough, England, UK, May 1965.

[14]Batchelor, G. K., and Gill, A. E., "Analysis of the Stability of Axisymmetric Jets," *Journal of Fluid Mechanics,* Vol. 14, 1962, pp. 529-551.

[15]Malik, M. R., and Orszag, S. A., "Efficient Computation of the Stability of Three-Dimensional Compressible Boundary Layers," AIAA 14th Fluid and Plasma Dynamics Conference, AIAA Paper 81-1277, Palo Alto, CA, June 1981.

Characterization of Droplet/Vapor/ Vortex Interactions in a Two-Dimensional Shear Layer

R. D. Hancock*
U.S. Air Force Wright Laboratory,
Wright-Patterson Air Force Base, Ohio 45433
and
L. P. Chin†
Systems Research Laboratories, Inc., Dayton, Ohio 45440

Introduction

TWO-PHASE flows are often difficult to characterize because of the complex interaction of the solid particles or liquid droplets and the gas. These flows become even more complicated when the fundamental characteristics of the particles or droplets change due to such processes as evaporation and combustion. These complex flows are commonplace in such devices as industrial burners, internal-combustion engines, and gas turbine combustors. In many cases, the droplet or particle sizes and velocities can be measured, and the gas velocity can also be determined using a variety of velocimetry techniques. However, little information is available on the vapor after it leaves the surface of the evaporating droplet.[1-4] This information is particularly important in combusting sprays because combustion typically takes place away from the surface of the droplet where the fuel-to-air ratio is appropriate.

The visualization technique presented in this Note is a new method for accurate visualization and prediction of the convective transport of vapor in two-phase flows. Water droplets are injected into a $TiCl_4$-laden gaseous flow where they evaporate. The water vapor reacts spontaneously with the $TiCl_4$ vapor to form micrometer-sized TiO_2 particles. The particles are sufficiently small to accelerate rapidly to the velocity of the carrier gas but are too large to diffuse readily. Thus, they are convected along the path that the water vapor follows as it leaves the droplets. The instantaneous locus of the TiO_2 particles is defined as a "vaporline" and can be visualized using Mie scattering. Although the technique for visualizing vaporlines is relatively simple, the physics required to interpret the vaporlines in terms of the droplet, vapor, and fluid interactions can be complicated. The goal of this study was to provide insight into the physics needed to understand and interpret vaporlines. Additionally, predictions from a computer model are presented that support the qualitative interpretation of the vaporline data.

Presented as Paper 93-0416 at the AIAA 31st Aerospace Sciences Meeting, Reno, NV, Jan. 11-14, 1993; received Feb. 10, 1993; revision received July 20, 1993; accepted for publication July 26, 1993.

*Captain, Wright Laboratory, WL/POSF Bldg. 490, 1790 Loop Road N. Member AIAA.

†Senior Research Engineer, 2800 Indian Ripple Road. Member AIAA.

Experimental

The experimental data presented in this Note were obtained in the two-dimensional shear-layer facility described in more detail elsewhere.[5] The splitter plate divides a 12.7-cm-square duct equally. Dry air was used in both airstreams. The gas velocities were set at 0.70 m/s and 0.35 m/s for the high- and low-speed sides of the flow giving localized Reynolds numbers of less than 1000. The higher-speed air was passed over a liquid $TiCl_4$ bath for collection of $TiCl_4$ vapor, as is done in reactive Mie scattering (rms).[6] For rms, two gaseous flows—one seeded with water vapor, the other with $TiCl_4$ vapor—must come in molecular contact. When the $TiCl_4$ reacts with the water vapor, TiO_2 particles are formed that act as light scatterers to mark the interaction of the two streams. The products of the $TiCl_4$ and H_2O reaction are HCl and TiO_2. The TiO_2 is a fine white powder that is quite inert, but the HCl can create problems because of its corrosive nature. The quantity of HCl produced is quite low, but a hood should always be used when trying to visualize a flow with $TiCl_4$.

Droplets were injected through a slot in the Plexiglas duct on the low-speed side of the flow. The droplets were ~60 μm in diameter and had sufficient momentum to cross the shear layer to the high-speed, $TiCl_4$-laden side of the flow. Micrometer-sized TiO_2 particles were formed as the water vapor mixed with the $TiCl_4$. The flowfield was illuminated by the 532-nm light output of a frequency-doubled Nd:YAG laser. Water droplets and the TiO_2 particles were the only scatters in the flowfield, and they could be easily distinguished by their 50:1, or greater, diameter ratio. Water-droplet injection was controlled using a droplet-on-demand generator that was driven by a piezoelectric crystal transducer.[7]

Vortices form at roughly 20 Hz for the undriven shear layer, but they are not as stable as desired for the collection of phase-locked measurements and photographs. Therefore, vortex formation was controlled by acoustically driving the low-speed airstream at 20 Hz. A 1% velocity fluctuation was introduced into the low-speed side of the flow due to the acoustic driving. The natural shear layer and driven shear layer are very similar in appearance, but the vortices in the driven shear layer are more controlled and equally spaced. The location of the water droplets and the entrainment of the water vapor into the individual vortices of the shear layer, as marked by TiO_2 particles, were recorded with a digitizing camera. The curve identified by the location of the TiO_2 particles at the instant of visualization is referred to as a vaporline.

Results and Discussion

A vaporline image of a two-dimensional shear layer in which a vortex is forming is shown in Fig. 1. The high-speed side of the flow is on the left and the low-speed side of the flow is on the right with flow from bottom to top. The left side of the flow is seeded with $TiCl_4$ vapor that reacts quickly and spontaneously with the water vapor from the droplets to form TiO_2 particles. Seven water droplets are visible in this particular image. The air on the left of the shear layer is moving faster than the droplets, and this causes the vapor to precede the droplets as they move downstream. Each droplet has a vaporline associated with it. More detailed analysis of images such as that shown in Fig. 1 led to the development of the schematic shown in Fig. 2 for describing the time and spatial development of the vaporlines.[5]

The vaporline schematic illustrates a specific case in which each droplet is introduced into a driven laminar flow at the same fre-